Long-range two-dimensional superstructure in the superconducting electron-doped cuprate Pr$_{0.88}$LaCe$_{0.12}$CuO$_4$

B. J. Campbell,[1,*] S. Rosenkranz,[2,†] H. J. Kang,[3] H. T. Stokes,[1] P. J. Chupas,[2,4] S. Komiya,[5] Y. Ando,[6] Shiliang Li,[7,8] and Pengcheng Dai[9]

[1]*Department of Physics and Astronomy, Brigham Young University, Provo, Utah 84602, USA*

[2]*Materials Science Division, Argonne National Laboratory, Argonne, Illinois 60439, USA*

[3]*Department of Physics and Astronomy, Clemson University, Clemson, South Carolina 29634, USA*

[4]*Advanced Photon Source, Argonne National Laboratory, Argonne, Illinois 60439, USA*

[5]*Central Research Institute of Electric Power Industry, Nagasaka, Yokosuka, Kanagawa 240-0196, Japan*

[6]*Institute of Scientific and Industrial Research, Osaka University, Ibaraki, Osaka 567-0047, Japan*

[7]*Beijing National Laboratory for Condensed Matter Physics, Institute of Physics, Chinese Academy of Sciences, Beijing 100190, China*

[8]*Collaborative Innovation Center of Quantum Matter, Beijing 100871, China*

[9]*Department of Physics and Astronomy, Rice University, Houston, Texas 77005, USA*

Utilizing single-crystal synchrotron x-ray scattering, we observe distorted CuO$_2$ planes in the electron-doped superconductor Pr$_{1-x}$LaCe$_x$CuO$_{4+\delta}$, $x = 0.12$. Resolution-limited rods of scattering are indicative of a long-range two-dimensional $2\sqrt{2} \times 2\sqrt{2}$ superstructure in the a-b plane, adhering to planar space-group symmetry $p4gm$, which is subject to stacking disorder perpendicular to the planes. This superstructure is present only in annealed, superconducting samples, but not in the as-grown, nonsuperconducting samples. These long-range distortions of the CuO$_2$ planes, which are generally considered to be detrimental to superconductivity, have avoided detection to date due to the challenges of observing and interpreting subtle diffuse-scattering features.

I. INTRODUCTION

The role of lattice-symmetry breaking [1] in the superconducting phases of high-T_C cuprates is a topic of great current interest. In addition to the influence of spin [2–4] and electronic correlations [5,6], structural distortions [7–10] and cation disorder [11,12] can strongly influence T_C in the hole-doped cuprates. The inverse correlation between T_C and the CuO$_2$ planar buckling angle in La$_{2-x}$Sr$_x$CuO$_4$ at fixed composition, for example, indicates that flat and square CuO$_2$ planes are preferable for high critical temperatures [7]. In addition, very recent evidence implicates charge order [13,14] and charge density waves [15,16] within the CuO$_2$ planes as important structural order parameters that compete with superconductivity.

For electron-doped cuprates with the T' structure, as-grown samples are generally not superconducting [17], though superconductivity can be reversibly induced by a high-temperature annealing procedure [18]. This process repairs defects present in the CuO$_2$ planes of as-grown samples due to slight Cu deficiencies [19] and leads to a separation into a defect-free superconducting majority phase and epitaxial intergrowths of a copper-free impurity phase [18–21]. While the resulting elimination of defects within the CuO$_2$ sheets clearly enhances superconductivity, the T_C values of these properly reduced electron-doped cuprates are still quite low compared to many hole-doped cuprates.

For T' cuprates with sufficiently small rare-earth ions, such as Gd$_2$CuO$_4$ or (Nd$_{1-y}$Tb$_y$)$_{1.85}$Ce$_{0.15}$CuO$_4$ ($y > 0.37$), superconductivity is completely suppressed by a three-dimensional superstructure involving in-plane rotations of the CuO$_2$ squares [22–24]. These observations lead one to wonder if intrinsic distortions of the CuO$_2$ sheets might also be suppressing T_C values in the superconducting T' compounds with larger rare-earth ions. In this paper, we report long-range two-dimensional superstructural distortions within the CuO$_2$ sheets of Pr$_{1-x}$LaCe$_x$CuO$_{4+\delta}$ (PLCCO) at $x = 0.12$, which appear only in the reduced samples that support superconductivity, and which have been difficult to detect in past work due to nearby scattering from the minority rare-earth sesquioxide phase and to a high level of superstructural stacking disorder.

II. RESULTS AND DISCUSSION

Single crystals of PLCCO (space group $I4/mmm$, $a_c = 3.98$ Å, $c_c = 12.3$ Å) were grown using the traveling-solvent floating-zone technique. Four sample batches were prepared from the same as-grown batch of PLCCO: as-grown nonsuperconducting (ag-NSC), reduced superconducting (r-SC), oxygenated nonsuperconducting (o-NSC), and re-reduced superconducting (r2-SC) crystals, as described by Kang *et al.* [19]. Single-crystal x-ray scattering experiments in both transmission and reflection geometries were performed at room temperature with 30 keV x rays at the BESSRC 11-ID-C and 11-ID-D beamlines of the Advanced Photon Source (APS) at Argonne National Laboratory. One- and two-dimensional reciprocal-space scans were performed using a Huber six-circle goniometer and either a Cyberstar or a Si-drift point detector, with energy discrimination to eliminate higher-order contamination from the monochromator. Reciprocal-lattice vectors labeled as $Q = (H,K,L)$ are defined here relative to the tetragonal lattice of the T' cuprate unless otherwise specified.

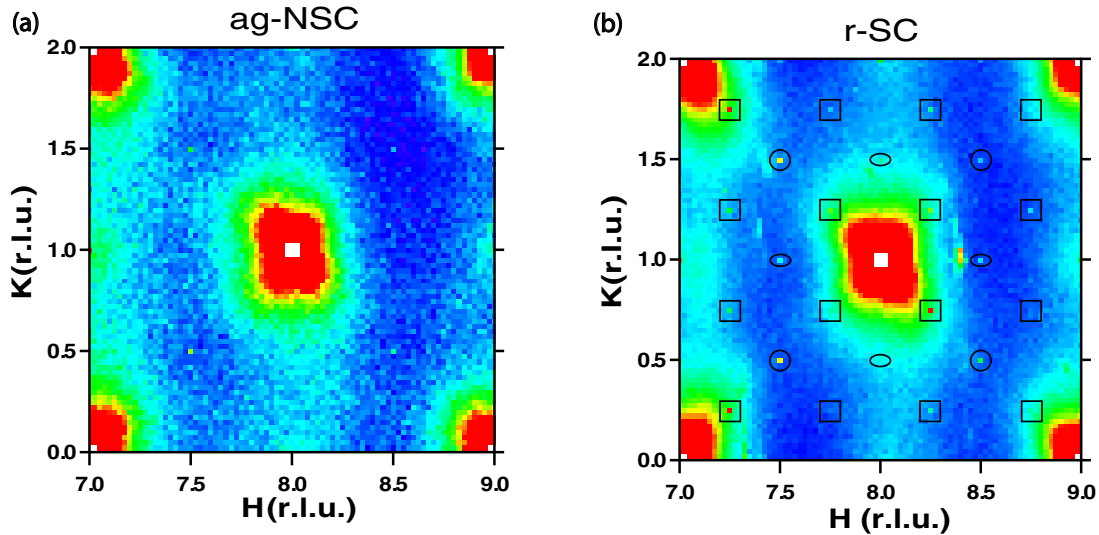*branton_campbell@byu.edu

†srosenkranz@anl.gov

FIG. 1. (Color online) Two-dimensional single-crystal x-ray diffuse scattering scan from the $L_c = 3$ reciprocal-space plane of the r-SC sample of PLCCO. Symbols are used to indicate visible signals at superlattice peak positions relative to the reciprocal lattice of the parent cuprate: circles for (1/2,1/2)-type peaks, ellipses for (1/2,0)-type peaks, and squares for (1/4,1/4)-type peaks. The concentrated intensity surrounding each of the intense Bragg reflections of the parent cuprate is thermal-diffuse scattering, and it is nominally identical among all of the samples studied. Superlattice intensities were only observed in the SC samples.

In the superconducting r-SC and r2-SC samples of PLCCO, two-dimensional diffuse-scattering measurements indicate the presence of superlattice peaks at the (1/4, 1/4)-, (1/2, 1/2)-, and (1/2, 0)-type positions, as shown in Fig. 1(b). These same peaks are absent in both the ag-NSC and o-NSC nonsuperconducting samples, except for very weak intensities at the (1/2, 1/2) positions in Fig. 1(a), which we verified to be second-order harmonic contamination from the monochromator and eliminated in subsequent measurements. A long L-scan through a superlattice position uncovers a series of weak but sharp diffraction peaks belonging to the C-type rare-earth-sesquioxide impurity phase, which forms thin epitaxial layers perpendicular to c^* within the r-SC and r2-SC samples [20]. The cubic lattice parameter of

the vacancy-ordered sesquioxide impurity (space group $Ia\bar{3}$, $a_s = 11.26$ Å) is very well matched to a $2\sqrt{2} \times 2\sqrt{2}$ supercell of the cuprate lattice within the a-b plane. Perpendicular to the CuO$_2$ sheets, however, a_s is roughly 10% smaller than c_c [20,21,25]. To avoid confusion, we will refer to the c^*-axis reciprocal-lattice coordinates of the cuprate and sesquioxide phases as L_c and L_s, respectively.

Long L scans were obtained at room temperature at a number of (1/4, 1/4)-, (1/2, 1/2)-, and (1/2, 0)-type superlattice positions. In addition to the expected impurity-phase reflections, which are very sharp, these scans reveal well-defined "needles" of diffuse scattering parallel to the c^* axis, which appear as a broadly structured background in Fig. 2(a). And like the impurity-phase peaks, they are observed
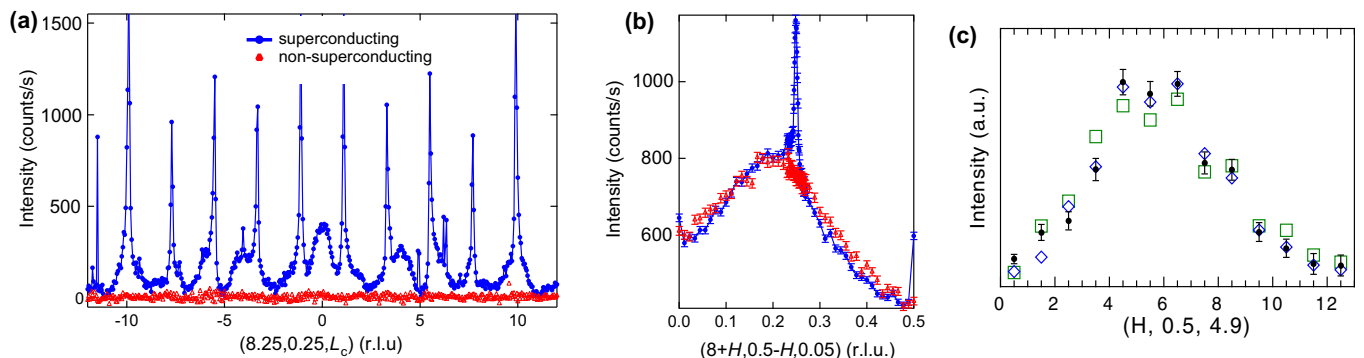

FIG. 2. (Color online) (a) Scans along $(8.25, 0.25, L_c)$ in the o-NSC (red) and r2-SC (blue) PLCCO samples. A modulated needle of diffuse scattering is apparent below a series of sharp sesquioxide impurity peaks. (b) Scans along $(8.0 + H, 0.5 - H, 0.05)$ in the same two samples. (c) Relative intensity trend of the diffuse needles located at positions $(H = n + 1/2, K = 1/2)$ for integers n in the range 0 to 12, where each closed black circle represents the amplitude of a Gaussian fit to an H scan through the corresponding needle at $L_c = 4.9$, and where blue diamonds and green squares indicate fitted values based on respective planar-distortion models A and B. The perpendicular scans in (a) and (b) intersect at their respective centers, both having peaks at $(8.25, 0.25, 0)$. The broad peak below the needle peak in (b) is thermal-diffuse scattering (TDS) associated with the parent $(8,0,0)$ Bragg peak. This TDS scattering was measured along lines offset from the diffuse needles and then subtracted from the needles to produce panel (a).

only in the reduced samples that exhibit low-temperature superconductivity. The superlattice intensities seen in Fig. 1(b) are actually the intersections of diffuse needles with the $L_c = 3$ plane, which is well separated from the nearest sesquioxide peaks at $L_c \approx 3.3$ ($L_s = 3$). The resolution-limited sharpness of the diffuse needles in the a^*-b^* plane, as shown in Fig. 2(b), indicates the presence of a long-range planar $2\sqrt{2} \times 2\sqrt{2}$ superstructure. Furthermore, the diffuse needles with substantial intensity exhibit modulations along their lengths that are roughly periodic and clearly commensurate with the c-axis cuprate lattice parameter, unambiguously demonstrating that the superstructure is a feature of the parent T' cuprate itself rather than a feature of the sesquioxide impurity phase. The impurity phase contributes apparent superlattice-peak intensities at (1/4, 1/4)- and (1/2, 0)-type positions only for odd values of L_s [20], which cannot explain the overall pattern of needle-intensity modulations. More importantly, the intraneedle modulation period matches the distance between neighboring CuO$_2$ sheets, so that we associate the diffuse needles with a superstructural distortion of the CuO$_2$ sheets.

Each closed black circle in Fig. 2(c) represents the amplitude of a Gaussian fit to an H-scan through the corresponding needle at $L_c = 4.9$, a value well separated from impurity peaks at $L_c = 4.4$ ($L_s = 4$) and from any second-order harmonic signal that might be present at $L_c = 5$. These relative needle intensities show an approximately quadratic dependence on the in-plane component of Q (call it $Q_\perp$) near the origin of the a^*-b^* plane, and they develop a more complex dependence

at higher values of $Q_\perp$. This is evidence of in-plane atomic displacements within the CuO$_2$ sheets, as opposed to some sort of oxygen ordering. In contrast, the individual needles [e.g., Fig. 2(a)] exhibit no marked intensity growth with increasing $|L_c|$, indicating that out-of-plane displacements are either absent or too small to detect.

Long L scans were collected along several hundred superlattice-needle lines, making it possible to study the intra-needle modulations in detail. First, we observed the modulation amplitudes to be much larger for (1/4,1/4,0)-type needles than for (1/2, 0)- or (1/2, 1/2)-type needles. Second, scans along several (1/4, 1/4)-type needles (shown in Fig. 3) reveal two distinct classes of (1/4, 1/4)-type needle modulations. The first class, illustrated in Fig. 3(a), includes needles that are located adjacent to planar parent-phase Bragg peaks with even values of $H + K$, which have modulations that peak at even values of L_c and which are easily identified by a peak at $L = 0$. The second class, illustrated in Fig. 3(b), includes needles located adjacent to parent-phase Bragg peaks with odd values of $H + K$, which have modulations that peak at odd values of L_c and which are easily identified by a trough at $L = 0$.

These modulation features are explained by the simplest possible stacking-disorder model. Because the planar supercell is eight times larger than the parent cell, there are eight different locations for the supercell origin, λ_1, of a given CuO$_2$ sheet relative to the supercell origin, λ_2, of an adjacent CuO$_2$ sheet. Of the two symmetry-unique choices for the relative origin separation, we assign probability α to the closer
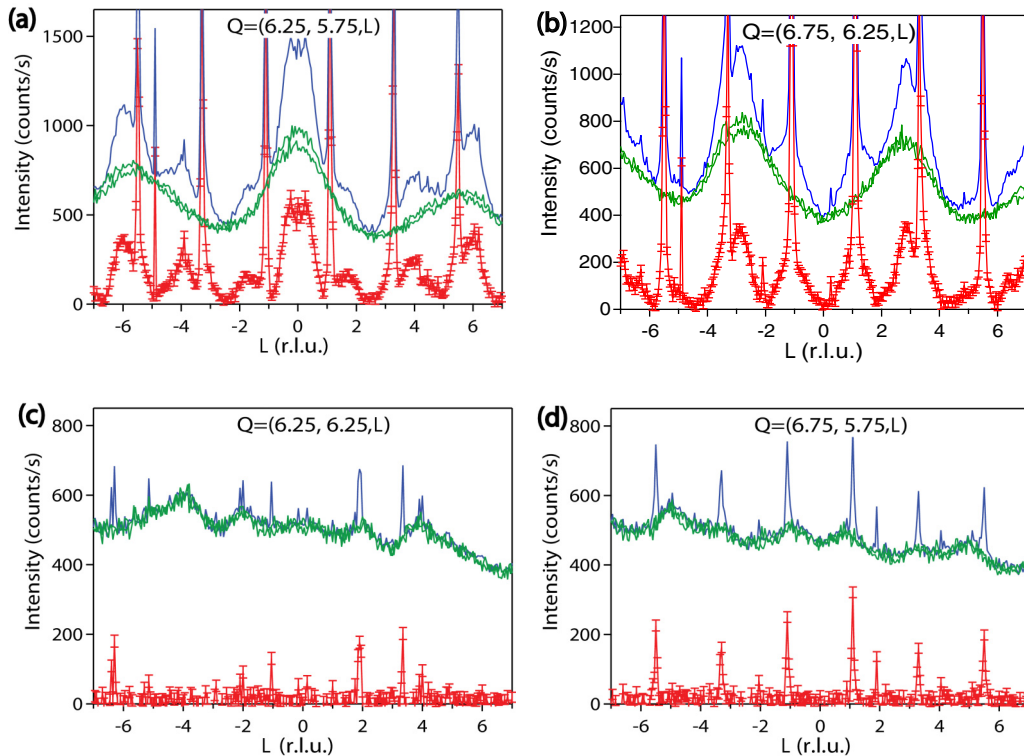

FIG. 3. (Color online) Blue indicates scans along the diffuse needles located at (a) (6.25,5.75,L_c), (b) (6.75,6.25,L_c), (c) (6.25,6.25,L_c), and (d) (6.75,5.75,L_c) over the range between $L_c = \pm 7$ in the r2-SC sample of PLCCO. Green indicates two TDS scans separated from the corresponding diffuse needle $|\Delta H| = |\Delta K| = 0.03$ r.l.u., one being slightly closer to the nearest parent Bragg peak and the other slightly farther away. Red indicates TDS-corrected diffuse-needle data, which were obtained by subtracting the average of the two green scans from the corresponding blue scan.

origin choice and probability $1 - \alpha$ to the more distant choice. The intensity modulations due to origin-shift correlations can then be computed as a probability-weighted average over all possible intersheet origin separation vectors [26]

$$I \propto \sum_{\lambda_1, \lambda_2} \langle e^{i \boldsymbol{Q} \cdot (\lambda_1 - \lambda_2)} \rangle. \tag{1}$$

Taking into account only nearest-neighbor correlations, Eq. (1) yields modulations of the form

$$I \propto 1 \pm (2\alpha - 1)\cos(\pi L_c) \tag{2}$$

for (1/4, 1/4)-type needles, where the "+" sign applies to needles near Bragg peaks with even values of $H + K$, and the "−" sign applies to needles near Bragg peaks with odd values of $H + K$. In contrast, (1/2, 0)- and (1/2, 1/2)-type needles receive zero intensity. This is precisely the pattern that we observe experimentally provided that small origin separations are favored over large ones for adjacent sheets (i.e., $\alpha > 1/2$). The fact that the peak/trough intensity ratios are quite high in Figs. 3(a) and 3(b) is evidence that nearest-neighbor origins are highly correlated (i.e., $\alpha \approx 1$). More detail is provided in the Appendix.

The ISODISTORT software [27] was used to explore distortions generated by the irreducible representations (irreps) of the parent $p4gm$ symmetry of the CuO$_2$ sheet at reciprocal-space points in the first Brillouin zone. We found that the $\Sigma(1/4, 1/4, 0)$-point irreps are required for obtaining the observed $2\sqrt{2} \times 2\sqrt{2}$ supercell, though there are a number of $M(1/2, 1/2, 0)$, $X(1/2, 0, 0)$, and $\Gamma(0, 0, 0)$-point irreps that can also contribute secondary order parameters to such a distortion. Of the four Σ-point irreps, only the first two (Σ_1 and Σ_2) are capable of in-plane displacements. The action of either the Σ_1 or Σ_2 irrep cleanly partitions the set of (1/4, 1/4)-type superlattice intensities into two distinct subsets. The first set contains peaks separated from the nearest parent Bragg peak by $\pm(1/4, -1/4)$, as represented by the scans in panels (a) and (b) of Fig. 3, while the second set contains peaks separated from the nearest parent Bragg peak by $\pm(1/4, +1/4)$, as represented by the scans in panels (c) and (d). Structure factor calculations show that for small displacements (<0.2 Å), the Σ_2 irrep parameters require the intensities of the second subset to approach zero in the vicinity of the $|H| = |K|$ diagonals of the parent reciprocal lattice, just as we observe in the figure. Because the Σ_1 irrep would have the opposite effect (the diagonal extinction of the first subset), its parameters can be ignored.

The Σ_2 irrep consists of rank-4 matrices, and the components of its four-dimensional order parameter correspond to the four symmetry-equivalent arms of the star of $\Sigma(1/4, 1/4, 0)$ in the first Brillouin zone, which are $(+1/4, +1/4, 0)$, $(-1/4, -1/4, 0)$, $(+1/4, -1/4, 0)$, and $(-1/4, +1/4, 0)$. The common shorthand notation for order parameters uses (a, b, c, d) to indicate that all four arms have different mode amplitudes, which also implies that they have different diffraction intensities. Similarly, $(a, 0, a, 0)$ indicates that the first and third arms have identical nonzero mode amplitudes and intensities while those of the other two arms are zero.

For Σ_2, there are five simple (i.e., single-parameter) forms that the order parameter can take, one of which

should capture the essential features of the planar distortion. They are $(a, 0, 0, 0)$, $(a, -a, 0, 0)$, $(a, 0, a, 0)$, $(0, a, a, 0)$, and $(a, -a, a, -a)$, each of which yields a distinct subgroup of the parent space-group symmetry and different structural degrees of freedom. A more complicated order parameter consistent with the observed supercell would be a superposition of these simple order parameters, though such fine structural details are not readily discernible by the present experiment due to the difficulty of measuring and interpreting the diffuse scattering pattern.

Because our high-resolution 2D reciprocal-space scans reveal no evidence of an orthorhombic (rectangular) splitting of the superlattice needle positions in the HK plane, we assume the distortion to be tetragonal (square), which is consistent with either $\Sigma_2(a, 0, a, 0)$ or $\Sigma_2(0, a, a, 0)$. Both of these order parameters generate a primitive $2\sqrt{2} \times 2\sqrt{2}$ supercell with space group $P4/mbm$ (planar group $p4gm$), though their respective supercell origins relative to the parent structure are different: $(0, 0, 0)$ and $(1/2, 1/2, 0)$. For simplicity, we refer to the distortions that arise from the $\Sigma_2(a, 0, a, 0)$ and $\Sigma_2(0, a, a, 0)$ order parameters as models A and B, respectively, which are illustrated in Fig. 4. Both of these order parameters enable an in-plane copper-displacement mode associated with local point-group irrep E_u and two in-plane oxygen-displacement modes associated with local point-group irreps B_{2u} and B_{3u}. These degrees of freedom support physically intuitive CuO$_2$ rotations and/or stretches in either model.

Model A has three symmetry-unique Cu sites and exhibits an alternating pattern of CuO$_2$ rotations and Jahn-Teller-like stretch modes that appears to be consistent with a checkerboard pattern of Cu^{1+} and Cu^{2+} charges. Model B, on the other hand, has only one symmetry-unique Cu site and presents a pattern of Jahn-Teller-like distortions with two long bonds and two short bonds per CuO$_2$ unit, somewhat like the distorted Pr$_{0.6}$Ca$_{0.4}$MnO$_3$ structure attributed to the presence of Zener polarons [28]. Via constraints, we were able to perform single-parameter structural refinements of models A and B against a limited number of relative needle intensities, as shown in Fig. 2(c). The fits, which included a flat-plate x-ray absorption correction and an isotropic Debye-Waller displacement factor, indicate maximum atomic displacements of about 0.15 Å. Surprisingly, models A and B yield nearly identical calculated intensity patterns, and are not likely to be distinguished by
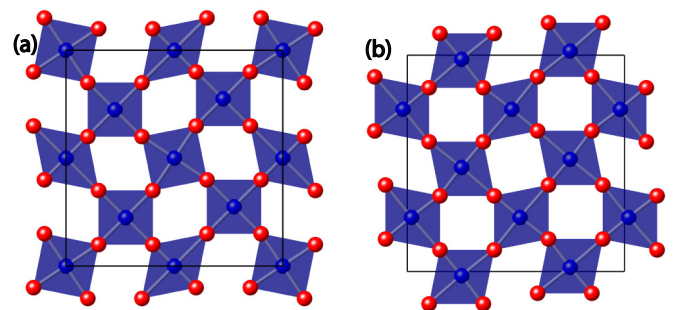

FIG. 4. (Color online) Illustrations of superstructural planar distortion models (a) A and (b) B of the CuO$_2$ sheets of PLCCO, both of which have planar symmetry $p4gm$. The distortion amplitudes have been exaggerated for visual clarity.

superlattice intensities. A local-structure probe may be more effective in differentiating the Cu environments of these two structures [29].

Purely displacive $2\sqrt{2} \times 2\sqrt{2}$ superstructures were reported by Krekels *et al.* in nonsuperconducting hole-doped cuprates from the tetragonal region of the $YBa_2Cu_3O_{6+x}$ phase diagram near $x = 0$ [30,31], with superlattice peaks also appearing as diffuse rods or needles. There, a model very similar to our model A was said to reproduce electron diffraction patterns better than oxygen-ordering models. However, single-crystal neutron diffraction data [32] have been interpreted by some [33] to support a 3D oxygen-ordering model for $YBa_2Cu_3O_{6.35}$. This could merely indicate different physical phenomena in different composition ranges. A single-crystal x-ray diffraction study [34] further reported evidence of a $2\sqrt{2} \times 2\sqrt{2}$ oxygen-ordered supercell in $NdBa_2Cu_3O_{6.5}$, though some of its authors supported the model of Krekels *et al.* for $YBa_2Cu_3O_6$ [35].

III. CONCLUSIONS

When superconductivity is reversibly enabled and disabled in electron-doped PLCCO via high-temperature annealing in respective reducing and oxidizing atmospheres, we observe the formation of long-range 2D superstructural distortions within the CuO_2 sheets of superconducting samples, but not in nonsuperconducting samples. The Q dependence of the interneedle intensity distribution provides unambiguous evidence that the superstructure is predominantly comprised of in-plane atomic displacements rather than an oxygen-vacancy ordering. The pattern of intraneedle intensity modulations makes it clear that the diffuse needles arise due to the formation of a superstructure within the CuO_2 sheets of the T' cuprate phase, and not due to some feature of the sesquioxide intergrowth layers. By restricting candidate structures according to their ability to reproduce the most distinctive features of the experimental diffuse-scattering distribution, we have also isolated viable distortion models. The absence of the planar distortions in nonsuperconducting samples is likely due to defect-induced frustration associated with Cu vacancies. Subsequent reduction heals these defects through the formation of the sesquioxide impurity phase and allows the now-clean CuO_2 sheets to lower their energy via distortion. Because of the relative difficulty of identifying and interpreting the subtle diffuse scattering from these rather large planar structural distortions, they have gone undetected in the superconducting phase until now. Because conventional wisdom dictates that any distortions of the CuO_2 sheets are likely to compete with the superconducting order parameter, we speculate that their presence might explain the systematically low critical temperatures of the family of electron-doped T' cuprates. Future work should seek to identify comparable diffuse scattering features in other superconducting members of this family.

ACKNOWLEDGMENTS

APPENDIX: SUPERCELL STACKING CORRELATIONS

Due to the body-centered relationship between adjacent CuO_2 sheets of a T' cuprate such as $Pr_{0.88}LaCe_{0.12}CuO_4$ (PLCCO), it is not possible for the origins of the planar $2\sqrt{2} \times 2\sqrt{2}$ supercells in these sheets to stack directly atop one another along the tetragonal **c** axis. Rather, the supercell origins in adjacent sheets must be offset along an in-plane direction, giving rise to multiple equally probable origin placements and stacking disorder. Figure 5 illustrates the probabilities of the symmetry-distinct candidate supercell origins in the nearest-neighbor and next-nearest-neighbor CuO_2 sheets of PLCCO.

The structure factor of a layered system subject to stacking disorder can be expressed in terms of the single-layer structure factor $F_0(\boldsymbol{H})$ and a probability-weighted average over the distribution of relative interlayer origin-separation vectors [26]. If λ_1 and λ_2 are vector variables that cycle over the origins of all layers, this average can be expressed as

$$I = |F_0(\boldsymbol{H})|^2 \sum_{\lambda_1, \lambda_2} \langle e^{2\pi i \boldsymbol{H} \cdot (\lambda_1 - \lambda_2)} \rangle, \quad \text{(A1)}$$

where $\boldsymbol{H} = (H, K, L)$ is a vector of the reciprocal superlattice, and the separation vector $\Delta\lambda = \lambda_1 - \lambda_2$ can be reduced modulo a vector of the direct-space sublattice. Executing the summation of Eq. (1) then yields modulations of the form

$$I \propto 1 + \sum_{n=1}^{\infty} T_n(H, K) \cos(n\pi L), \quad \text{(A2)}$$

where $n = 1$ accounts for correlations in the nearest-neighbor sheet, $n = 2$ accounts for correlations in the next-nearest-neighbor sheet, and so on. For a given diffuse needle located at in-plane position (H, K), the coefficient $T_n(H, K)$ provides the amplitude and sign of the nth harmonic of the intensity modulation, which depends only on the positions and probabilities of the candidate origin sites in the nth sheet. A needle with a large nonzero value of T_n should have an observable modulation period of $\Delta L = 2/n$ provided that it also has a substantial single-layer structure factor. A positive value of T_n yields a modulation that peaks at $L = 0$, and a negative value of T_n yields a modulation that dips at $L = 0$.

If we initially consider only nearest-neighbor correlations, then $\Delta\lambda = (0, 0, 1/2) + \boldsymbol{s}$, where the in-plane vector $\boldsymbol{s}$ points to any of the sites with collective probability α or α' in Fig. 5. The value of T_1 in Eq. (A2) then evaluates to $+1/2$ for needles passing through allowed parent Bragg positions, to $-1/2$ for
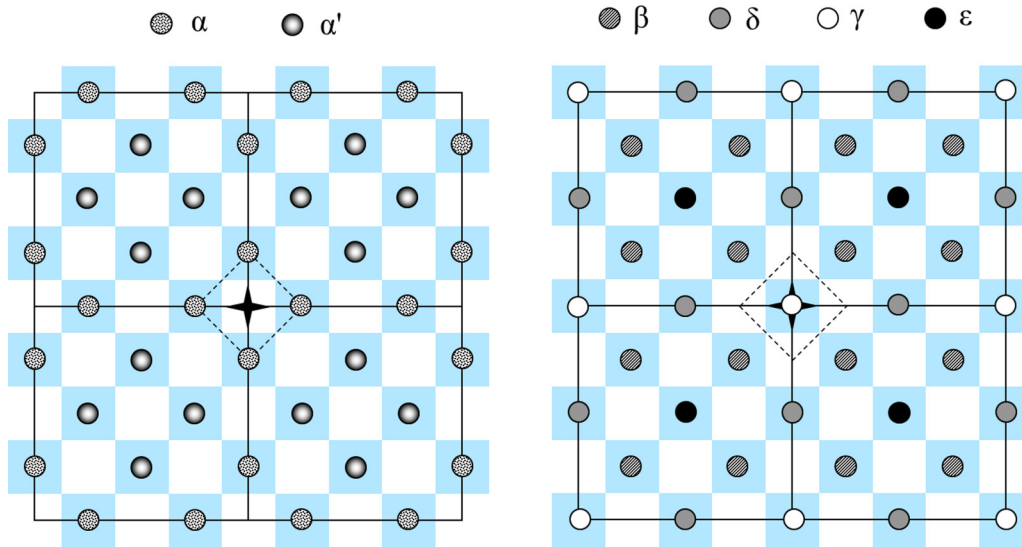
FIG. 5. (Color online) Illustration of the symmetry-distinct supercell-origin options in the nearest-neighbor (left) and next-nearest-neighbor (right) sheets of PLCCO. The dashed and solid lines delineate the parent cuprate cell and the $2\sqrt{2} \times 2\sqrt{2}$ supercell, respectively, while blue squares represent individual CuO_2 units. The four-arm star symbol at the center of each sheet indicates the location of the supercell origin in the primary ($n = 0$) CuO_2 sheet, while small circles indicate the eight possible supercell-origin locations in a neighboring sheet. Observe that the supercell origin in the nearest-neighbor sheet cannot lie directly on top of the origin in the primary sheet due to the body-centered relationship between adjacent sheets. The Greek symbols in the legend at the top of the figure represent the probabilities of finding the supercell origin at the corresponding sites. Thus, the collective probability that the origin will lie in one of the speckled-circle sites in the nearest-neighbor sheet is α. Because the placement probabilities in a given sheet must add up to 1, we have $\alpha + \alpha' = 1$ in the nearest-neighbor sheet and $\beta + \delta + \gamma + \epsilon = 1$ in the next-nearest-neighbor sheet. A strictly random distribution would have $\alpha/4 = \alpha'/4 = \beta/4 = \delta/2 = \gamma = \epsilon = 1/8$, so that all origin sites are equally probable.

needles passing through forbidden parent Bragg positions, to 0 for needles at (1/2,0)- and (1/2,1/2)-type positions, to $+(2\alpha - 1)$ for (1/4,1/4)-type needles near integer positions (in parent coordinates) where $H + K$ is even, and to $-(2\alpha - 1)$ for (1/4,1/4)-type needles near integer positions where $H + K$ is odd.

The diffuse needles passing through the allowed parent Bragg positions are buried beneath the Bragg-peak tails, and are therefore difficult to observe. The diffuse needles passing through forbidden parent Bragg positions should be modulated, but are weak if present at all, possibly because the superstructure has a weak single-layer structure factor at these points. In contrast, the diffuse needles passing through the (1/4,1/4)-type positions are quite strong and uniformly adhere to the pattern expected for nearest-neighbor correlations with $\alpha \approx +1$. The fact that the observed modulations are not cleanly periodic, but rather appear to be multiplied by a lower-frequency envelope function, is evidence that the rare-earth atoms above and below each CuO_2 sheet (approximately 0.15 c from the sheet) also play a role.

The diffuse needles passing through the (1/2,1/2)- and (1/2,0)-type positions are generally much weaker than the

(1/4, 1/4)-type needles, and are somewhat difficult to distinguish in our data from the broad Lorentzian tails of the thin impurity layers. But Fig. 8(b) of Ref. [20] shows that some (1/2, 1/2)- and (1/2, 0)-type needles exhibit weak peaks at $L = 0$. Because $T_1 = 0$ for these needles, nearest-neighbor correlations cannot be responsible, though next-nearest-neighbor-sheet correlations may be. For next-nearest-neighbor correlations, the value of T_2 in Eq. (1) evaluates to zero for all allowed and forbidden parent Bragg positions, to $1 - 2\beta$ for (1/2,1/2)-type positions, to $1 - \beta - 2\delta$ for (1/2,0)-type positions, and to $1 - \beta - \delta - 2\gamma$ for all (1/4,1/4)-type positions. The $L = 0$ peaks of Ref. [20] then support a model in which β and δ have values smaller than would be expected for a random stacking, which means that these sites are disfavored. Given the strength of the nearest-neighbor correlations (i.e., the large value of α), which favors small interlayer origin-separation vectors, it seems unlikely that ϵ would be substantially nonzero. So there is evidence that γ is larger than would be expected for a random stacking, and that the preferred site for the supercell origin in the next-nearest-neighbor sheet lies directly above the supercell origin in the primary ($n = 0$) sheet.

[1] M. Vojta, Adv. Phys. **58**, 699 (2009).

[2] J. M. Tranquada, B. J. Sternlieb, J. D. Axe, Y. Nakamura, and S. Uchida, Nature (London) **375**, 561 (1995).

[3] S. A. Kivelson, E. Fradkin, and V. J. Emery, Nature (London) **393**, 550 (1998).

[4] S. A. Kivelson, I. P. Bindloss, E. Fradkin, V. Oganesyan, J. M. Tranquada, A. Kapitulnik, and C. Howald, Rev. Mod. Phys. **75**, 1201 (2003).

[5] R. Daou, J. Chang, D. LeBoeuf, O. Cyr-Choiniere, F. Laliberte, N. Doiron-Leyraud, B. J. Ramshaw, R. Liang, D. A. Bonn, W. N. Hardy, and L. Taillefer, Nature (London) **463**, 519 (2010).

[6] M. J. Lawler, K. Fujita, J. Lee, A. R. Schmidt, Y. Kohsaka, C. K. Kim, H. Eisaki, S. Uchida, J. C. Davis, J. P. Sethna, and E.-A. Kim, Nature (London) **466**, 347 (2010).

[7] H. Takahashi, H. Shaked, B. A. Hunter, P. G. Radaelli, R. L. Hitterman, D. G. Hinks, and J. D. Jorgensen, Phys. Rev. B **50**, 3221 (1994).

[8] B. Buchner, M. Breuer, A. Freimuth, and A. P. Kampf, Phys. Rev. Lett. **73**, 1841 (1994).

[9] W. E. Pickett, Phys. Rev. Lett. **78**, 1960 (1997).

[10] O. Chmaissem, J. D. Jorgensen, S. Short, A. Knizhnik, Y. Eckstein, and H. Shaked, Nature (London) **397**, 45 (1999).

[11] H. Eisaki, N. Kaneko, D. L. Feng, A. Damascelli, P. K. Mang, K. M. Shen, Z.-X. Shen, and M. Greven, Phys. Rev. B **69**, 064512 (2004).

[12] K. Fujita, T. Noda, K. M. Kojima, H. Eisaki, and S. Uchida, Phys. Rev. Lett. **95**, 097006 (2005).

[13] E. H. da Silva Neto, P. Aynajian, A. Frano, R. Comin, E. Schierle, E. Weschke, A. Gyenis, J. Wen, J. Schneeloch, Z. Xu, S. Ono, G. Gu, M. Le Tacon, and A. Yazdani, Science **343**, 393 (2014).

[14] T. Wu, H. Mayaffre, S. Krämer, M. Horvatić, C. Berthier, P. L. Kuhns, A. P. Reyes, R. Liang, W. N. Hardy, D. A. Bonn, and M. H. Julien, Nat. Commun. **4**, 2113 (2013).

[15] G. Ghiringhelli, M. Le Tacon, M. Minola, S. Blanco-Canosa, C. Mazzoli, N. B. Brookes, G. M. De Luca, A. Frano, D. G. Hawthorn, F. He, T. Loew, M. Moretti Sala, D. C. Peets, M. Salluzzo, E. Schierle, R. Sutarto, G. A. Sawatzky, E. Weschke, B. Keimer, and L. Braicovich, Science **337**, 821 (2012).

[16] J. Chang, E. Blackburn, A. T. Holmes, N. B. Christensen, J. Larsen, J. Mesot, R. Liang, D. A. Bonn, W. N. Hardy, A. Watenphul, M. v. Zimmermann, E. M. Forgan, and S. M. Hayden, Nat. Phys. **8**, 871 (2012).

[17] N. P. Armitage, P. Fournier, and R. L. Greene, Rev. Mod. Phys. **82**, 2421 (2010).

[18] K. Kurahashi, H. Matsushita, M. Fujita, and K. Yamada, J. Phys. Soc. Jpn. **71**, 910 (2002).

[19] H. J. Kang, P. Dai, B. J. Campbell, P. J. Chupas, S. Rosenkranz, P. L. Lee, Q. Huang, S. Li, S. Komiya, and Y. Ando, Nat. Mater. **6**, 224 (2007).

[20] P. K. Mang, S. Larochelle, A. Mehta, O. P. Vajk, A. S. Erickson, L. Lu, W. J. L. Buyers, A. F. Marshall, K. Prokes, and M. Greven, Phys. Rev. B **70**, 094507 (2004).

[21] H. Kimura, Y. Noda, F. Sato, K. Tsuda, K. Kurahashi, T. Uefuji, M. Fujita, and K. Yamada, J. Phys. Soc. Jpn. **74**, 2282 (2005).

[22] M. Braden, P. Adelmann, P. Schweiss, and T. Woisczyk, Phys. Rev. B **53**, R2975 (1996).

[23] M. Braden, W. Paulus, A. Cousson, P. Vigoureux, G. Heger, A. Goukassov, P. Bourges, and D. Petitgrand, Europhys. Lett. **25**, 625 (1994).

[24] P. Vigoureux, M. Braden, A. Gukasov, W. Paulus, P. Bourges, A. Cousson, D. Petitgrand, J. P. Lauriat, M. Meven, S. N. Barilo, D. I. Zhigunov, P. Adelamann, and G. Heger, Physica C **273**, 239 (1997).

[25] M. Matsuura, P. Dai, H. J. Kang, J. W. Lynn, D. N. Argyriou, K. Prokes, Y. Onose, and Y. Tokura, Phys. Rev. B **68**, 144503 (2003).

[26] B. J. Campbell, Z. Kristallogr. **220**, 1088 (2005).

[27] B. J. Campbell, H. T. Stokes, D. E. Tanner, and D. M. Hatch, J. Appl. Crystallogr. **39**, 607 (2006).

[28] A. Daoud-Aladine, J. Rodriguez-Carvajal, L. Pinsard-Gaudart, M. T. Fernandez-Diaz, and A. Revcolevschi, Phys. Rev. Lett. **89**, 097205 (2002).

[29] S. J. L. Billinge and T. Egami, Phys. Rev. B **47**, 14386 (1993).

[30] T. Krekels, T. S. Shi, J. Reyes-Gasga, G. Van Tendeloo, J. Van Landuyt, and S. Amelinckx, Physica C **167**, 677 (1990).

[31] T. Krekels, S. Kaesche, and G. Van Tendeloo, Physica C **248**, 317 (1995).

[32] R. Sonntag, D. Hohlwein, T. Bruckel, and G. Collin, Phys. Rev. Lett. **66**, 1497 (1991).

[33] A. A. Aligia and J. M. Eroles, Physica C **272**, 197 (1996).

[34] T. Frello, N. H. Andersen, J. Madsen, A. B. Abrahamsen, M. v. Zimmermann, T. Niemoller, J. R. Schneider, and Th. Wolf, Phys. Rev. B **61**, R9253 (2000).

[35] M. v. Zimmermann, J. R. Schneider, T. Frello, N. H. Andersen, J. Madsen, M. Kall, H. F. Poulsen, R. Liang, P. Dosanjh, and W. N. Hardy, Phys. Rev. B **68**, 104515 (2003).